inorganics

MDPI

Article

Chiral, Heterometallic Lanthanide–Transition Metal Complexes by Design

Anders Øwre [1], Morten Vinum [1], Michal Kern [2], Joris van Slageren [2], Jesper Bendix [1,*] and Mauro Perfetti [1,*]

[1] Department of Chemistry, University of Copenhagen, Universitetparken 5, 2100 Copenhagen, Danmark; dtz872@alumni.ku.dk (A.Ø.); morten.vinum@chem.ku.dk (M.V.)

[2] Institut für Physikalische Chemie, Universität Stuttgart, Pfaffenwaldring 55, D-70569 Stuttgart, Germany; m.kern@ipc.uni-stuttgart.de (M.K.); ipcjosl@ipc.uni-stuttgart.de (J.v.S.)

* Correspondence: bendix@kiku.dk (J.B.); mauro.perfetti@chem.ku.dk (M.P.)

Received: 15 June 2018; Accepted: 17 July 2018; Published: 19 July 2018

Abstract: Achieving control over coordination geometries in lanthanide complexes remains a challenge to the coordination chemist. This is particularly the case in the field of molecule-based magnetism, where barriers for magnetic relaxation processes as well as tunneling pathways are strongly influenced by the lanthanide coordination geometry. Addressing the challenge of design of 4f-element coordination environments, the ubiquitous Ln(hfac)$_3$ moieties have been shown to be applicable as Lewis acids coordinating transition metal acetylacetonates facially leading to simple, chiral lanthanide–transition metal heterodinuclear complexes. The broad scope of this approach is illustrated by the synthesis of a range of such complexes **LnM**: LnM(hfac)$_3$(μ_2-acac-O,O,O′)$_3$ (Ln = La, Pr, Gd; M = Cr, Fe, Ga), with approximate three-fold symmetry. The complexes have been crystallographically characterized and exhibit polymorphism for some combinations of 4f and 3d metal centers. However, an isostructural set of systems spanning several lanthanides which exhibit spontaneous resolution in the orthorhombic Sohncke space group $P2_12_12_1$ is presented here. The electronic structure and ensuing magnetic properties have been studied by EPR spectroscopy and magnetometry. The **GdFe**, **PrFe**, and **PrCr** complexes exhibit ferromagnetic coupling, while **GdCr** exhibits antiferromagnetic coupling. **GdGa** exhibits slow relaxation of the magnetization in applied static fields.

Keywords: lanthanides; transition metals; anisotropy; magnetism; magnetic coupling; geometric design

1. Introduction

Recent years have seen a revival of lanthanide coordination chemistry, partially fueled by their promising magnetic properties [1–3]. Thus, mononuclear lanthanide complexes, polynuclear lanthanide complexes, lanthanides coordinating organic radicals, and mixed 3d–4f metal complexes have all yielded single molecule magnets [2–6]. Among them, only few exhibit chirality [7–10]. In many regards, lanthanide-based systems outperform molecular magnets based on transition metals, but in the context of magnetic properties, the flexibility of the lanthanide ions concerning coordination numbers and coordination geometries complicates matters in more than one sense. Firstly, as the ligand field splitting in lanthanide complexes is energetically subordinate to the interelectronic repulsion and spin-orbit coupling, the coordination geometries and ensuing ligand fields become determining for the magnetic properties. Hence, tuning of magnetic properties requires a degree of tailoring the coordination environments, which is often difficult to realize for lanthanides. Secondly, the pliant geometries around lanthanide ions hamper the design of highly symmetrical systems, which can act as building blocks for extended structures since any symmetry imposed by multidentate ligands is easily

broken. Thus, although crystallographically strictly axial, trigonal, and tetragonal [11–20] lanthanide complexes have been obtained by the use of structure-directing ligands, these systems typically feature coordinatively saturated lanthanide centers with no obvious avenues towards extended structures which preserve the tailored symmetry. Addressing this challenge, we forward a simple route towards heterobinuclear transition metal–lanthanide complexes with near-axial symmetry.

The hexafluoroacetylacetonate (hfac) complexes of the trivalent lanthanide ions are ubiquitous starting materials. While the homoleptic neutral entities $Ln(hfac)_3$ are unknown in the condensed phase, many neutral heteroleptic complexes $Ln(hfac)_3L_n$ with lanthanide coordination numbers ranging from 7 to 10 [21–24] have been structurally characterized. Among these, eightfold coordination dominates as exemplified by the aquo-complexes $Ln(hfac)_3(H_2O)_2$ [25] (cf. Figure 1a). Indeed, the Lewis acidic fragment $Ln(hfac)_3$ has been employed as a building block for several structures by ligation of bidentate transition metal complexes creating heterometallic bi- and polynuclear systems in a systematic fashion [26,27] where one simple system is illustrated in Figure 1b [28]. However, to date, only a single example of a triply bridged system based on the $Ln(hfac)_3$ fragment, namely $CuLa(\mu_2\text{-acac-}O,O,O')_2(\mu\text{-}H_2O)(hfac)_3$ (acac = acetylacetonate), entailing nine-coordination of the large La^{3+} ion, has been reported (cf. Figure 1c) [29].

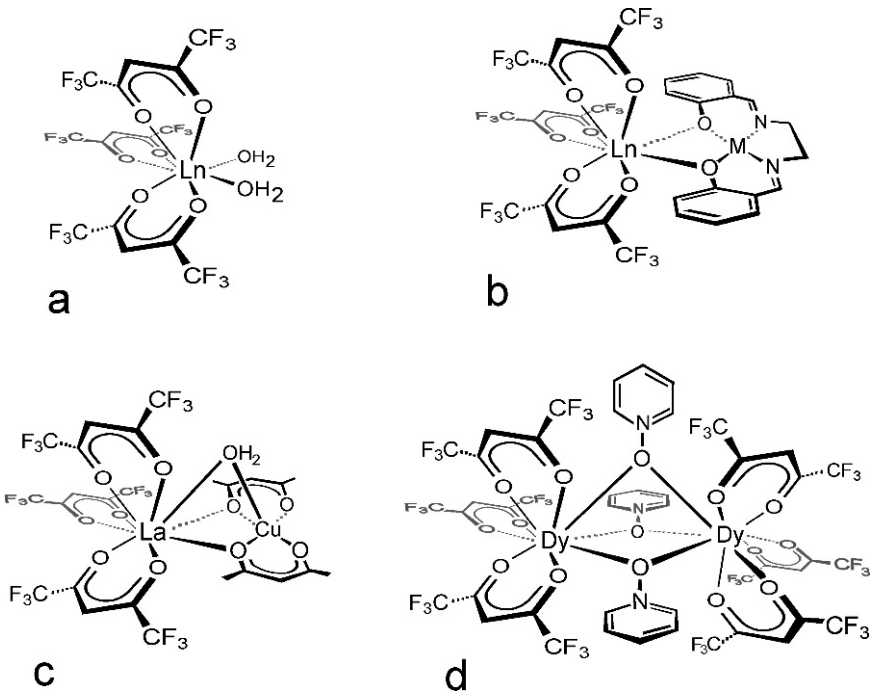

Figure 1. Schematic structures of (**a**) the $Ln(hfac)_3(H_2O)_2$ precursor; (**b**) $Ln(hfac)_3$ ligated by bidentate Schiff-base complexes (M = Cu, Ni); (**c**) the hitherto sole structurally characterized example of a triply bridged $Ln(hfac)_3$—transitional metal binuclear complex; and (**d**) triple bridging in homodinuclear $(hfac)_3Dy(\mu\text{-}PyO)_3Dy(hfac)_3$.

Common to the previously studied systems is the geometric incompatibility of the transition metal and the lanthanide fragments, which inevitably lowers the overall symmetry to C_1. Notable is also the system [(NiL)Gd(hfac)$_2$(EtOH)] (L = μ_2-1,1,1-tris(*N*-salicylideneaminomethyl)ethane) [30], where the trifold symmetric Schiff-base ligand provides too much steric encumbrance to preserve three hfac ligands on the lanthanide. Inspired by the above-mentioned $CuLa(\mu\text{-acac})_2(\mu\text{-}H_2O)(hfac)_3$ and by examples of triple bridging between two $Ln(hfac)_3$ fragments in, e.g., $(hfac)_3Ln(\mu\text{-}PyO)_3Ln(hfac)_3$ (Ln = Eu, Dy; cf. Figure 1d) [31], we decided to pursue the possibility of facial coordination of sterically undemanding, threefold symmetric transition metal complexes terminated in hard oxygen donor

ligands to $Ln(hfac)_3$ fragments aiming at threefold symmetric dinuclear systems. This approach necessitates the use of non-competing and hence weakly coordinating solvents, imposing some restrictions on the suitable transition metal building blocks. Evidently, uncharged complexes with three mono-anionic, bidentate ligands meet both the symmetry and solubility requirements and pose an obvious starting point. Indeed, this approach proved feasible and focusing on the pervasive tris-acetylacetonates of the trivalent transition metal ions, a subset of such systems which indeed conforms to the designed threefold pseudosymmetry is presented here (Figure 2).

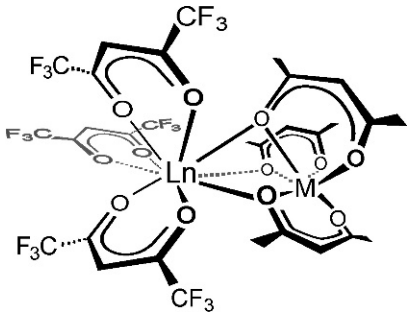

Figure 2. Schematic structure of the targeted mixed lanthanide–transition metal acetylacetonates, $LnM(hfac)_3(\mu\text{-acac})_3$ (Ln = La, Pr, Gd; M = Cr, Fe, Ga).

2. Results and Discussion

Synthesis of the face-sharing mixed 3d–4f metal acetylacetonates $LnM(hfac)_3(\mu\text{-acac})_3$ proceeds in a facile manner by dehydration of the $Ln(hfac)_3(H_2O)_2$ precursor through azeotropic distillation with, e.g., benzene in the presence of the transition metal acetylacetonate. In this fashion, triply bridged binuclear complexes have been accessed with Ln = La through Tb. The method provides moderate to good yields (30–84%) of well-crystalline products, which, if needed, can be recrystallized from non-coordinating solvents (e.g., chloroform, hexane...). The heterobinuclear complexes exhibit polymorphism and in the present contribution, we have chosen to focus on an orthorhombic phase which has been obtained pure for Ln = La, Pr, Nd, Sm, Eu, Gd, and Tb with M = Cr, Fe, Ga. This phase can be reproducibly obtained by use of the crystallization procedure described in the experimental section. Other phases belonging to the monoclinic and triclinic crystal systems have been observed for some combinations of 3d and 4f metals, but these will not be discussed here.

The heterobinuclear complexes $LnM(hfac)_3(\mu\text{-acac})_3$ were obtained spontaneously resolved in the Sohncke space group $P2_12_12_1$. The 65 Sohncke space groups (often called chiral space groups) contain only rotation or screw axes. They are thus the only groups in which an enantiopure compound crystallize, and hence also the only groups allowing spontaneous resolution. The resolution occurs by conglomerate formation as demonstrated by structure determination of both enantiomorphs of **PrFe** (cf. Supplementary Materials). Illustrations of the molecular structure and packing of Λ,Δ-**GdFe** are given in Figure 3. Tables S1–S3 report the relevant crystallographic data for all the described complexes.

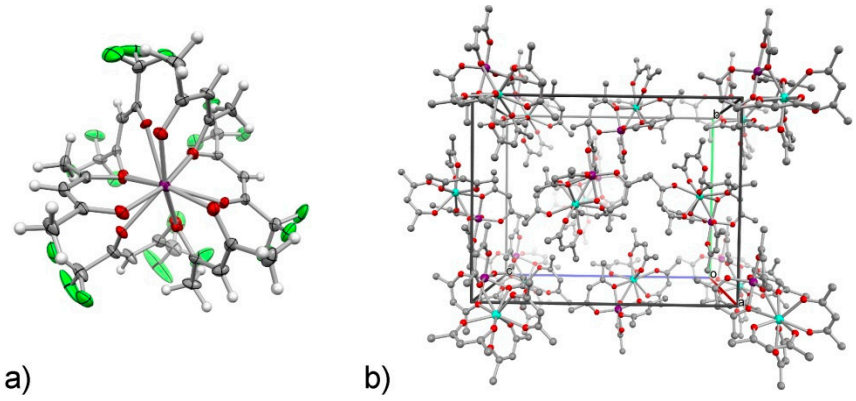

Figure 3. (**a**) The molecular structure of Λ,Δ-**GdFe** in the solid state viewed along the approximate threefold axis of the single molecule constituting the asymmetric unit. Thermal ellipsoids represent a probability level of 50%. Disorder in one of the CF_3 groups has been omitted for clarity. (**b**) Packing view along the crystallographic *b*-axis, emphasizing the four different molecular orientations dictated by the molecules residing at general positions. Hydrogen and fluorine atoms have been omitted for clarity. Color coding: Fe: purple, F: light green, O: red, C: gray, Gd: turquoise. For alternate views cf. Supplementary Materials, Figure S1. For metrics cf. Table 1.

Notably, of the more than 850 known structures containing the $Ln(hfac)_3$ fragment only 38 crystallize in one of the Sohncke space groups and only two heterobimetallic $Ln(hfac)_3$ complexes, both of which are Cu(II)-containing chains, have been found to show spontaneous resolution [32,33]. It must be concluded that the weak dispersion forces from the heavily fluorinated $Ln(hfac)_3$ fragments are not efficient in enforcing chiral packings. In line with this conclusion, the majority of short inter-molecular contacts in the packing of **LnM** involve the acetylacetonate ligands, alone or in addition to the hexafluoroacetylacetonate ligands (see Supplementary Materials, Figure S2 for details). In all cases, the ligand sphere around the d- or p-block metal is ordered, but in some cases the coordination sphere around the lanthanide is disordered with both helicities represented. In the systems **LaFe**, **PrFe**, and **GdFe**, no disorder is observed and the chirality of the two metal centers is invariably opposite. We hypothesize that the size of the light-metal fragment governs the locking of the relative configurations around the metal centers and the concomitant order in the lanthanide coordination sphere. The metric parameters for select combinations of metal ions are collected in Table 1.

Table 1. Metric data for select $LnM(hfac)_3(\mu\text{-}acac)_3$ complexes.

Complex	$M–O_{acac}$/Å	$Ln–O_{hfac}$/Å	$Ln–O_{acac}$/Å	$<O_3>–<LnO_3>–<MO_3>$/° [a]	Ln–M/Å
LaCr	1.943–1.971	2.454–2.530	2.649–2.661	176.10	3.420
LaFe	1.962–2.049	2.457–2.503	2.629–2.636	177.21	3.514
PrCr	1.940–1.968	2.415–2.470	2.607–2.628	176.05	3.380
PrFe	1.958–2.045	2.426–2.467	2.587–2.606	177.38	3.471
PrGa	1.918–1.983	2.406–2.459	2.587–2.605	176.63	3.425
GdCr	1.936–1.966	2.336–2.399	2.535–2.565	176.18	3.321
GdFe	1.953–2.051	2.356–2.419	2.513–2.538	177.59	3.406
GdGa	1.921–1.983	2.336–2.406	2.516–2.530	176.80	3.355

[a] $<O_3>$ denotes the centroid defined by the three remote oxygen ligators of the hfac ligands, $<LnO_3>$ the centroid defined by the three bridging oxygen ligators of the acetylacetonate ligands, and $<MO_3>$ the centroid of the three terminal oxygen ligators of the acetylacetonate ligands.

In the first column of Table 1, bond length ranges are given for the d-block metals, including Ga. The geometric perturbation of the $M(acac)_3$ complexes upon ligation to the lanthanides is quite moderate as reflected by the minor changes in bond length from the parent systems: 1.9413–1.9645 Å (for $Cr(acac)_3$), 1.986–2.004 Å (for $Fe(acac)_3$), and 1.941–1.964 Å (for $Ga(acac)_3$). Evident is also the

higher geometric pliancy of Ga(III), and especially Fe(III) as compared to Cr(III), which is expected on the basis of the strong preference of Cr(III) for regular octahedral coordination. The second and third columns of Table 1 summarize the coordination geometry around the lanthanide ions. The observed contraction of ca. 6% in Ln–O_{acac} distances upon going from La to Gd is slightly accentuated over the corresponding contraction of the Ln–O_{hfac} distances. Again, the geometric rigidity of $Cr(acac)_3$ differentiates this metalloligand from the iron and gallium analogs resulting in longer Ln–O_{acac} bonds for the Cr(III) systems.

Although the binuclear complexes do not have crystallographic threefold symmetry, they approximate this situation quite closely. Thus, angles between centroids of the three-oxygen donor faces of the distant hfac-ligator atoms, the bridging acac-ligator atoms, and the terminal acac-ligator atoms range from 176.10° to 177.59°, indicating near co-linearity between the approximate threefold axes of the metal centers. The intermetallic distances span the interval 3.321–3.514 Å with distinct dependence on the nature of both metal centers as also reflected in the first coordination sphere bond distances (vide supra). Despite the only partial charge on the bridging donor atoms, the intermetallic distances are relatively short compared to other triply bridged lanthanide–transition metal complexes as illustrated in Figure 4. The relative proximity of the metal ions as well as the possibility of obtaining isostructural members of the series with diamagnetic centers at either position renders these systems well-suited for the investigation of magnetic properties, in particular 3d–4f magnetic interactions.

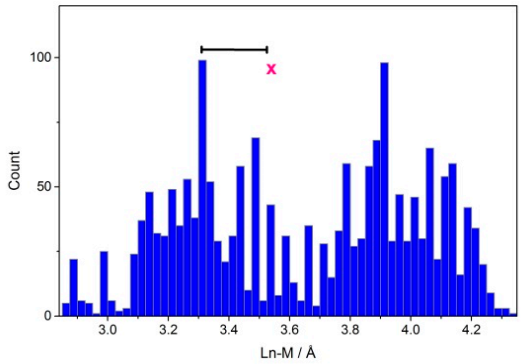

Figure 4. Distribution of lanthanide–transition metal distances for structurally characterized, triply bridged polynuclear systems. The bar indicates the range for the present La, Pr, and Gd systems. The cross indicates the average value for all triply bridged La–transition metal structures. The data are based on entries in CSD ver. 5.39.

The magnetic properties of all these compounds were investigated using dc and ac magnetometry. In Figure 5a, we report the χT product of all the investigated derivatives. The room temperature values of all the samples are consistent with the expected Curie constants for independent paramagnetic ions: **LaCr**: 2.04 (1.88); **LaFe**: 4.33 (4.38); **GdCr**: 9.55 (9.76); **GdFe**: 12.27 (12.26); **GdGa**: 7.76 (7.88); **PrCr**: 3.40 (3.48); **PrFe**: 5.89 (5.98); and **PrGa**: 1.69 (1.60). The χT product of **LaFe**, **LaCr**, and **GdGa** exhibits a small decrease on lowering temperature due to the relatively small magnetic anisotropy of both the trivalent transition metal ions and of the half-filled Gd^{3+} ion (cf. Supplementary Materials Figures S3 and S4). This allows a simple qualitative evaluation of the nature of the coupling that instead dominates the shape of the χT curves of the **GdM** (M = Ga, Fe, or Cr) derivatives: ferromagnetic (FM) in **GdFe** and antiferromagnetic (AFM) in **GdCr**. The nature of the coupling is more difficult to extract at a glance for the complexes containing Pr^{3+} due to its pronounced magnetic anisotropy. However, the low-temperature value of the χT product of **PrGa** (Figure 5a) goes to zero when the temperature is decreased, and the magnetization curves (Figure S5a) almost coincide at all temperatures, suggesting that the effect of the ligands is to stabilize the diamagnetic $m_J = 0$ ground state of Pr^{3+}. No hysteresis was observed in any of the samples at the lowest accessible temperature (1.8 K).

Simulation and parametrization of the magnetic data was performed using a Hamiltonian with the general expression:

$$\mathcal{H} = \sum_{i=1}^{n} \{\mu_B g_i H \cdot \hat{S}_i + D_i \hat{S}_{zi}^2\} + j\, \hat{S}_1 \cdot \hat{S}_2 \quad (1)$$

where the first summation runs over all the paramagnetic centers and contains the Zeeman interaction and Zero Field Splitting (ZFS). The second term, only used for complexes containing two paramagnetic ions, is an isotropic ferromagnetic ($j < 0$) or antiferromagnetic ($j > 0$) coupling [34]. For Pr^{3+}, the S quantum number in Equation (1) was replaced with the total angular momentum of the ground multiplet $J = 4$.

The parameters employed in the simulations are reported in Table 2. The errors in the parameter values were estimated to be on the last digit reported in Table 2. The evaluation was obtained varying the relevant parameters in the simulations and monitoring the resultant change in the reproduction of the data.

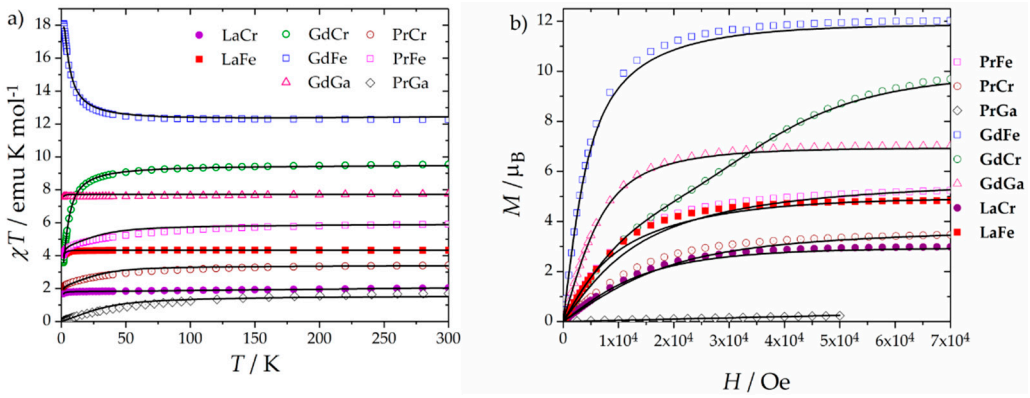

Figure 5. (**a**) Temperature behavior of the χT product of all the synthetized samples in an applied field of 1 kOe. (**b**) Magnetization curves recorded at 1.8 K. Symbols are experimental data, solid lines are simulations (see text). For additional variable temperature magnetization data see Supplementary Materials, Figures S3–S5.

Table 2. Zero Field Splitting (ZFS) parameters, g factors, and j coupling extracted from the dc magnetic measurements.

Sample	g_{Ln}	g_M	D_{Ln}/cm^{-1}	D_M/cm^{-1}	j/cm^{-1}
LaFe	-	1.991	-	−0.75	-
LaCr	-	1.965	-	−0.98	-
GdGa *	1.980	-	0.0465	-	-
GdFe	1.980	1.991	0.0465	−0.75	−0.38
GdCr	1.980	1.965	0.0465	−0.98	+0.78
PrGa	4/5	-	80	-	-
PrFe	4/5	1.991	80	−0.75	−0.25
PrCr	4/5	1.965	80	−0.98	−1.2

* Combined fit of EPR and magnetic data.

For **LaCr** and **LaFe**, an axial ZFS parameter (D) and an isotropic g factor were sufficient to reproduce the shape of both the χT and magnetization curves. The simulations of **LaFe**, **LaCr**, and **GdGa** did not allow for a unique determination of the sign of the ZFS. However, previous studies on $Cr(acac)_3$ and $Fe(acac)_3$ suggest a negative ZFS [35,36]; thus, we adopted that sign. As expected, the half-filled Fe^{3+} ion has a lower magnetic anisotropy and a g factor closer to 2 compared to the Cr^{3+} ion. The small anisotropy expected in **GdGa** required the use of a more sensitive technique to be accurately unraveled. We thus performed X-band EPR spectroscopy, obtaining the spectrum reported

in Figure 6. The simulation provided an estimation of the magnitude of the ZFS but not its sign (the magnetic measurements on **GdCr** and **GdFe** suggest a positive ZFS, *vide infra*).

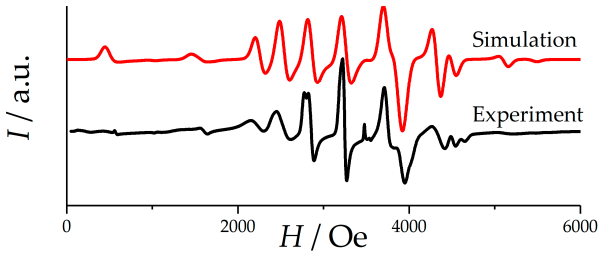

Figure 6. X-band EPR spectrum of **GdGa** at room temperature in the solid state.

The ZFS parameters and g factors obtained for the mono-paramagnetic complexes were fixed for the simulation of the poly-paramagnetic species, allowing for the extraction of the coupling constants reported in Table 2. For the **GdCr** and **GdFe** derivatives, a positive ZFS of Gd^{3+} was found to yield an improved goodness of the simulation compared to the negative case. The coupling in **LnFe** is significantly weaker than the one in **LnCr** for both **Ln** = Gd and Pr. The characteristic feature of the AFM coupling in **GdCr** (the only derivative that exhibits AFM coupling) is the step-like shape of the magnetization curve in Figure 5: indeed, a field of ca. 26.2 kOe is required to force the magnetic moments to be aligned with the field. A similar behavior with a spin rearrangement corresponding to a ferri-to-ferromagnetic transition at a comparable field was observed both by susceptometry and XMCD for the fluoride-bridged [$Dy(hfac)_3(H_2O)$–$CrF_2(py)_4$–$Dy(hfac)_3(NO_3)$] [37]. The magnitude of the coupling constants is well-comparable with other lanthanide–transition metal complexes connected by monoatomic bridges [38,39].

The magnetic anisotropy of Pr^{3+} could not be fully modelled with the available data; thus, we tentatively simulated it using a large positive D parameter (80 cm^{-1}) to mimic the diamagnetic ground state and an isotropic Landé factor (g_J = 4/5). The introduction of a coupling term allowed for satisfactory reproduction of the magnetic behavior of both **PrCr** and **PrFe**, revealing FM coupling in both compounds.

The ac measurements conducted on all the samples evidenced slow relaxation only in **GdGa**, reported in Figure S6 (B = 0–5000 Oe). The field scan at 1.8 K revealed the presence of a double peak in the imaginary part of the magnetic susceptibility (χ''), corresponding to two active relaxation processes (Figure S6b), as previously observed in a Gd–EDTA complex. [40] The available experimental frequency window allowed us only to monitor the slow process. A temperature scan with an optimum field (Figure S7) of 4000 Oe reveals that the complex exhibits a single relaxation time up to 2.8 K, conversely to Gd–EDTA. [40] The origin of the slow relaxation can be attributed either to quantum tunneling (QT) or to a phonon bottleneck since they have a similar ac response. [41] The field and temperature dependence of the slow process was consequently parametrized using the theoretical field dependence predicted for a single QT process (Figures S8 and S9) [41,42]. The extracted widths of the relaxation time ($0.31 < \alpha < 0.62$, Figure S10) provide further evidence that the QT regime persists up to 2.8 K since this process is particularly sensitive to strains and disorder [43].

3. Materials and Methods

3.1. Chemicals

All chemicals and solvents were purchased from commercial sources and used without further purification. All the syntheses were performed in open air. [$Ln(hfac)_3 \cdot x(H_2O)_2$] (Ln = La, Pr, Gd) ($x$ = 2, 3) were synthesized starting from the respective lanthanide oxides by modified literature methods [44]. [$M(acac)_3$] (M = Cr, Fe) were synthesized from transition metal salts according to the known procedures [45,46] while an adjusted procedure was used for M = Ga based on the synthesis

of [Fe(acac)$_3$]. The bulk samples used for the magnetic characterizations were verified by powder X-ray diffraction to be phase pure with diffractograms matching the theoretical ones for the $P2_12_12_1$ structures (Supplementary Materials, Figures S11–S18).

3.2. Synthesis

Synthesis of [La(hfac)$_3$Cr(acac)$_3$] (**LaCr**). La(hfac)$_3$·3H$_2$O (203.5 mg, 0.25 mmol) was boiled close to dryness while stirring in 20 mL of toluene in an Erlenmeyer flask. A new portion of 10 mL of toluene was added, and the solution was again boiled close to dryness. This was repeated two times yielding a pale yellow-brown solution. After the last portion of toluene had been boiled almost dry, the heat was turned off and a solution of [Cr(acac)$_3$] (69.9 mg, 0.20 mmol) in 5 mL of dichloromethane was slowly added to the hot (ca. 60 °C) reaction mixture causing an immediate boil off of dichloromethane. The resulting purple solution was allowed to cool down to room temperature (RT) without stirring, whereupon 10 mL of petroleum spirit was added, and the solution was filtered through a glass frit to remove any unreacted compounds. The solution was transferred to a crystallization bowl with a lid and stored in a refrigerator overnight to yield dark purple crystals of **LaCr**. To enhance the quality of the crystals, the crude product was recrystallized by boiling in 20 mL of n-heptane, filtering the solution, and then storing it in a refrigerator overnight. Yield: ~53%. Anal. Calcd. for **LaCr** ($C_{30}H_{24}CrF_{18}LaO_{12}$, molecular weight (MW) = 1109.40 g·mol^{-1}): C, 32.48%; H, 2.18%. Found: C, 32.48%; H, 2.45%.

Synthesis of [La(hfac)$_3$Fe(acac)$_3$] (**LaFe**). **LaFe** was synthesized using a procedure similar to **LaCr** with the replacement of [Cr(acac)$_3$] by [Fe(acac)$_3$] (70.6 mg, 0.20 mmol) producing dark red crystals. Yield: ~63%. Anal. Calcd. for **LaFe** ($C_{30}H_{24}F_{18}FeLaO_{12}$, MW = 1116.33 g·mol^{-1}): C, 32.36%; H, 2.17%. Found: C, 32.45%; H, 1.92%.

Synthesis of [Pr(hfac)$_3$Cr(acac)$_3$] (**PrCr**). **PrCr** was synthesized using a procedure similar to **LaCr** with the replacement of La(hfac)$_3$·3H$_2$O by Pr(hfac)$_3$·3H$_2$O (204.0 mg, 0.25 mmol) producing dark purple crystals. Yield: ~37%. Anal. Calcd. for **PrCr** ($C_{30}H_{24}CrF_{18}O_{12}Pr$, MW = 1111.40 g·mol^{-1}): C, 32.42%; H, 2.18%. Found: C, 32.46%; H, 2.00%.

Synthesis of [Pr(hfac)$_3$Fe(acac)$_3$] (**PrFe**). **PrFe** was synthesized using a procedure similar to **LaCr** with the replacement of La(hfac)$_3$·3H$_2$O by Pr(hfac)$_3$·3H$_2$O (204.0 mg, 0.25 mmol) and [Cr(acac)$_3$] by [Fe(acac)$_3$] (70.6 mg, 0.20 mmol) producing dark red crystals. Yield: ~30%. Anal. Calcd. for **PrFe** ($C_{30}H_{24}F_{18}FeO_{12}Pr$, MW = 1115.25 g·mol^{-1}): C, 32.31%; H, 2.18%. Found: C, 32.67%; H, 2.26%.

Synthesis of [Pr(hfac)$_3$Ga(acac)$_3$] (**PrGa**). **PrGa** was synthesized using a procedure similar to **LaCr** with the replacement of La(hfac)$_3$·3H$_2$O by Pr(hfac)$_3$·3H$_2$O (204.0 mg, 0.25 mmol) and [Cr(acac)$_3$] by [Ga(acac)$_3$] (73.4 mg, 0.20 mmol) producing faintly coloured yellow-green crystals. Yield: 35%. Anal. Calcd. for **PrGa** ($C_{30}H_{24}F_{18}GaO_{12}Pr$, MW = 1129.12 g·mol^{-1}): C, 31.91%; H, 2.14%. Found: C, 31.86%; H, 2.28%.

Synthesis of [Gd(hfac)$_3$Cr(acac)$_3$] (**GdCr**). **GdCr** was synthesized using a procedure similar to **LaCr** with the replacement of La(hfac)$_3$·3H$_2$O by Gd(hfac)$_3$·2H$_2$O (203.6 mg, 0.25 mmol) producing dark purple crystals. Yield: ~60%. Anal. Calcd. for **GdCr** ($C_{30}H_{24}CrF_{18}GdO_{12}$, MW = 1127.74 g·mol^{-1}): C, 31.95%; H, 2.15%. Found: C, 32.50%; H, 1.90%.

Synthesis of [Gd(hfac)$_3$Fe(acac)$_3$] (**GdFe**). **GdFe** was synthesized using a procedure similar to **LaCr** with the replacement of La(hfac)$_3$·3H$_2$O by Gd(hfac)$_3$·2H$_2$O (203.6 mg, 0.25 mmol) and [Cr(acac)$_3$] by [Fe(acac)$_3$] (70.6 mg, 0.20 mmol) producing dark red crystals. Yield: ~84%. Anal. Calcd. for **GdFe** ($C_{30}H_{24}F_{18}FeGdO_{12}$, MW = 1131.59 g·mol^{-1}): C, 31.84%; H, 2.14%. Found: C, 31.81%; H, 2.30%.

Synthesis of [Gd(hfac)$_3$Ga(acac)$_3$] (**GdGa**). **GdGa** was synthesized using a procedure similar to **LaCr** with the replacement of La(hfac)$_3$·3H$_2$O by Gd(hfac)$_3$·2H$_2$O (203.6 mg, 0.25 mmol) and [Cr(acac)$_3$] by [Ga(acac)$_3$] (73.4 mg, 0.20 mmol) producing faintly coloured sandy crystals. Yield: ~52%. Anal. Calcd. for **GdGa** ($C_{30}H_{24}F_{18}GaGdO_{12}$, MW = 1145.46 g·mol^{-1}): C, 31.45%; H, 2.11%. Found: C, 31.49%; H, 1.93%.

3.3. Single Crystal X-ray Diffraction Measurements

Single-crystal X-ray diffraction data were collected on a D8 VENTURE diffractometer (Bruker AXS, Karlsruhe, Germany) equipped with Mo Kα high brilliance IμS radiation (λ = 0.71073 Å), a multilayer X-ray mirror, a PHOTON 100 CMOS detector (Bruker AXS, Karlsruhe, Germany), and a low-temperature controller (Oxford Cryosystems, Oxford, UK). Crystals were mounted on loops made of Kapton. The diffractometer was controlled using the *SAINT* program as implemented in the APEX2 software package. Intensity data were corrected for absorption using the multi-scan method implemented in *SADABS*. The structures were solved using Olex2 by means of the olex2.structure solution program using a quasi-E charge flipping algorithm refined with the olex2.refine refinement package using Gauss–Newton minimization. Racemic twin refinements were carried out on all structures with a Flack parameter deviating more than 3 esds. from zero; in all cases, the crystals were determined not to be twinned with final Flack parameters equal to zero. For the structures with disordered hfac ligands, Shelx ISOR and DFIX restraints were applied to ensure chemically sensible metrics of the hfac ligands.

3.4. Powder X-ray Diffraction Measurements

Powder X-ray diffraction data were collected at room temperature on a D8 ADVANCE powder diffractometer (Bruker AXS, Karlsruhe, Germany) operating in a 2θ-θ configuration using Cu Kα radiation (λ = 1.5418 Å).

3.5. Magnetic Measurements

EPR spectra of **GdGa** were recorded on a microcrystalline powder sample using a Bruker Elexsys E500 equipped with a Bruker ER 4116 DM dual-mode cavity, an EIP 538B frequency counter and an ER035M NMR Gauss meter (Bruker Biospin, Rheinstetten, Germany). Effects related to crystallites' preferential orientation were dimmed mediating 90 spectra recorded at different orientations. Ac and dc magnetometry measurements were performed using a Quantum Design MPMS-XL7 SQUID magnetometer (Quantum Design, Darmstadt, Germany). The samples were measured as pressed pellets wrapped into teflon. The data were corrected for diamagnetism using Pascal's constants [47].

3.6. Simulations

All the simulations of the dc magnetic data were obtained using the Easy Spin package [48] of *MATLAB*. The ac susceptibility was fitted using a home-written program in *MATLAB*.

4. Conclusions and Outlook

A systematic building-block approach towards chiral and nearly axial heterobinuclear 3d–4f complexes has been forwarded. By employing sterically undemanding, threefold symmetric transition metal complexes it was found to be possible to extend the chemistry based on the $Ln(hfac)_3$ fragment to encompass triply bridged systems with nine-coordinate lanthanide centers. The resulting systems provide for relatively short 3d–4f distances (3.320–3.514 Å) and concomitant easily quantifiable magnetic interactions. The class of systems introduced here are amenable to extension towards other transition metal building blocks. Such investigations are currently being undertaken, and it has already been verified that other motifs based on, e.g., Ru(III), Re(V) and Co(III) complexes are applicable. It is noteworthy that the crystallization as conglomerates and ensuing spontaneous resolution provides a rare avenue towards chiral $Ln(hfac)_3$ fragments with potential for complete resolution based on adducts with robust chiral transition metal complexes.

Supplementary Materials: The following are available online at http://www.mdpi.com/2304-6740/6/3/72/s1: Tables S1–S3: Crystallographic data for the La-, Gd- and Pr-complexes, Checkcif for alternate enantiomorph of **PrFe**, Figure S1: Alternate views of the packing in **GdFe**, Figure S2: Shortest intermolecular interactions in the packing of **GdFe**, Figures S3–S5: Magnetization curves of **LaM**, **GdM**, and **PrM** recorded at T = 1.8, 5, and 10 K, Figures S6–S10: Ac susceptibility of **GdGa**, Figure S11–S18: Powder X-ray diffractograms of **LaCr, LaFe**, **GdCr**, **GdFe**, **GdGa, PrCr**, **PrFe**, and **PrGa**, Check cif files, and cif files.

Author Contributions: A.Ø., J.B., and M.V. synthetized the compounds and performed the chemical characterization. M.K. and J.v.S. facilitated the magnetic characterization. M.P. performed the magnetic characterization and data analysis. J.B. conceived and designed the project. The paper was written by A.Ø., J.B., and M.P. with inputs from all the authors.

Funding: This research was funded by the Independent Research Fund Denmark (#8021-00410B) and the Velux Foundations.

Conflicts of Interest: The authors declare no conflict of interest.

References

1. Goodwin, C.A.; Ortu, F.; Reta, D.; Chilton, N.F.; Mills, D.P. Molecular magnetic hysteresis at 60 kelvin in dysprosocenium. *Nature* **2017**, *548*, 439–442. [CrossRef] [PubMed]
2. McAdams, S.G.; Ariciu, A.-M.; Kostopoulos, A.K.; Walsh, J.P.; Tuna, F. Molecular single-ion magnets based on lanthanides and actinides: Design considerations and new advances in the context of quantum technologies. *Coord. Chem. Rev.* **2017**, *346*, 216–239. [CrossRef]
3. Layfield, R.A.; Murugesu, M. *Lanthanides and Actinides in Molecular Magnetism*; John Wiley & Sons: Hoboken, NJ, USA, 2015.
4. Sessoli, R.; Powell, A.K. Strategies towards single molecule magnets based on lanthanide ions. *Coord. Chem. Rev.* **2009**, *253*, 2328–2341. [CrossRef]
5. Woodruff, D.N.; Winpenny, R.E.; Layfield, R.A. Lanthanide single-molecule magnets. *Chem. Rev.* **2013**, *113*, 5110–5148. [CrossRef] [PubMed]
6. Pointillart, F.; Cador, O.; Le Guennic, B.; Ouahab, L. Uncommon lanthanide ions in purely 4f single molecule magnets. *Coord. Chem. Rev.* **2017**, *346*, 150–175. [CrossRef]
7. Wang, Y.; Li, X.L.; Wang, T.W.; Song, Y.; You, X.Z. Slow relaxation processes and single-ion magnetic behaviors in Dysprosium-containing complexes. *Inorg. Chem.* **2009**, *49*, 969–976. [CrossRef] [PubMed]
8. Li, X.L.; Chen, C.L.; Gao, Y.L.; Liu, X.L.; Feng, X.L.; Gui, Y.H.; Fang, S.M. Modulation of Homochiral Dy^{III} Complexes: Single Molecule Magnets with Ferroelectric Properties. *Chem. Eur. J.* **2012**, *18*, 14632–14637. [CrossRef] [PubMed]
9. Lin, P.H.; Korobov, I.; Wernsdorfer, W.; Ungur, L.; Chibotaru, L.F.; Murugesu, M. A rare μ_4-O Centred Dy_4 Tetrahedron with Coordination Induced Local Chirality and Single Molecule Magnet Behaviour. *Eur. J. Inorg. Chem.* **2011**, *10*, 1535–1539. [CrossRef]
10. Mihalcea, I.; Perfetti, M.; Pineider, F.; Tesi, L.; Mereacre, V.; Wilhelm, F.; Rogalev, A.; Anson, C.E.; Powell, A.K.; Sessoli, R. Spin Helicity in Chiral Lanthanide Chains. *Inorg. Chem.* **2016**, *55*, 10068–10074. [CrossRef] [PubMed]
11. Flanagan, B.M.; Bernhardt, P.V.; Krausz, E.R.; Lüthi, S.R.; Riley, M.J. A ligand-field analysis of the trensal (H_3trensal = 2,2′,2″-tris(salicylideneimino)triethylamine) ligand. An application of the angular overlap model to lanthanides. *Inorg. Chem.* **2002**, *41*, 5024–5033. [CrossRef] [PubMed]
12. Pedersen, K.S.; Dreiser, J.; Weihe, H.; Sibille, R.; Johannesen, H.V.; Sørensen, M.A.; Nielsen, B.E.; Sigrist, M.; Mutka, H.; Rols, S. Design of single-molecule magnets: Insufficiency of the anisotropy barrier as the sole criterion. *Inorg. Chem.* **2015**, *54*, 7600–7606. [CrossRef] [PubMed]
13. Pedersen, K.S.; Ungur, L.; Sigrist, M.; Sundt, A.; Schau-Magnussen, M.; Vieru, V.; Mutka, H.; Rols, S.; Weihe, H.; Waldmann, O. Modifying the properties of 4f single-ion magnets by peripheral ligand functionalisation. *Chem. Sci.* **2014**, *5*, 1650–1660. [CrossRef]
14. Perfetti, M.; Lucaccini, E.; Sorace, L.; Costes, J.P.; Sessoli, R. Determination of magnetic anisotropy in the lntrensal complexes (Ln = Tb, Dy, Er) by torque magnetometry. *Inorg. Chem.* **2015**, *54*, 3090–3092. [CrossRef] [PubMed]

15. Lucaccini, E.; Baldoví, J.J.; Chelazzi, L.; Barra, A.-L.; Grepioni, F.; Costes, J.-P.; Sorace, L. Electronic structure and magnetic anisotropy in lanthanoid single-ion magnets with C_3 symmetry: The Ln(trenovan) series. *Inorg. Chem.* **2017**, *56*, 4728–4738. [CrossRef] [PubMed]
16. Clemente-Juan, J.M.; Coronado, E.; Gaita-Ariño, A. Magnetic polyoxometalates: From molecular magnetism to molecular spintronics and quantum computing. *Chem. Soc. Rev.* **2012**, *41*, 7464–7478. [CrossRef] [PubMed]
17. Baldoví, J.J.; Cardona-Serra, S.; Clemente-Juan, J.M.; Coronado, E.; Gaita-Ariño, A.; Palii, A. Rational design of single-ion magnets and spin qubits based on mononuclear lanthanoid complexes. *Inorg. Chem.* **2012**, *51*, 12565–12574. [CrossRef] [PubMed]
18. Ishikawa, N.; Sugita, M.; Wernsdorfer, W. Quantum tunneling of magnetization in lanthanide single-molecule magnets: Bis(phthalocyaninato)terbium and bis(phthalocyaninato)dysprosium anions. *Angew. Chem. Int. Ed.* **2005**, *44*, 2931–2935. [CrossRef] [PubMed]
19. Sørensen, M.A.; Hansen, U.B.; Perfetti, M.; Pedersen, K.S.; Bartolomé, E.; Simeoni, G.G.; Mutka, H.; Rols, S.; Jeong, M.; Zivkovic, I.; et al. Chemical tunnel-splitting-engineering in a dysprosium-based molecular nanomagnet. *Nat. Commun.* **2018**, *9*, 1292. [CrossRef] [PubMed]
20. Sørensen, M.A.; Weihe, H.; Vinum, M.G.; Mortensen, J.S.; Doerrer, L.H.; Bendix, J. Imposing high-symmetry and tuneable geometry on lanthanide centres with chelating Pt and Pd metalloligands. *Chem. Sci.* **2017**, *8*, 3566–3575. [CrossRef]
21. Benelli, C.; Caneschi, A.; Gatteschi, D.; Pardi, L.; Rey, P. Structure and magnetic properties of linear chain complexes of rare earth ions (Gadolinium, Europium) with nitronyl nitroxides. *Inorg. Chem.* **1989**, *28*, 275–280. [CrossRef]
22. Gleizes, A.N.; Senocq, F.; Julve, M.; Sanz, J.L.; Kuzmina, N.; Troyanov, S.; Malkerova, I.; Alikhanyan, A.; Ryazanov, M.; Rogachev, A.; et al. Heterobimetallic single-source precursors for MOCVD. Synthesis and characterization of volatile mixed ligand complexes of Lanthanides, Barium and Magnesium beta-diketonates with d-element containing ligands. *J. Phys. IV* **1999**, *9*, 943–951.
23. Evans, W.J.; Giarikos, D.G.; Johnston, M.A.; Greci, M.A.; Ziller, J.W. Reactivity of the europium hexafluoroacetylacetonate (hfac) complex, Eu(hfac)$_3$(diglyme), and related analogs with potassium: Formation of the fluoride hfac "ate" complexes, [LnF(hfac)$_3$K(diglyme)]$_2$. *J. Chem. Soc. Dalton Trans.* **2002**, 520–526. [CrossRef]
24. Sun, O.; Gao, T.; Sun, J.; Li, G.; Li, H.; Xu, H.; Wang, C.; Yan, P. A series of lanthanide(III) complexes constructed from schiff base and β-diketonate ligands. *CrystEngComm* **2014**, *16*, 10460–10468. [CrossRef]
25. Kennedy, F.; Shavaleev, N.M.; Koullourou, T.; Bell, Z.R.; Jeffery, J.C.; Faulkner, S.; Ward, M.D. Sensitised near-infrared luminescence from lanthanide(III) centres using Re(I) and Pt(II) diimine complexes as energy donors in d–f dinuclear complexes based on 2,3-bis(2-pyridyl)pyrazine. *Dalton Trans.* **2007**, 1492–1499. [CrossRef] [PubMed]
26. Gleizes, A.; Julve, M.; Kuzmina, N.; Alikhanyan, A.; Lloret, F.; Malkerova, I.; Sanz, J.L.; Senocq, F. Heterobimetallic d–f metal complexes as potential single-source precursors for mocvd: Structure and thermodynamic study of the sublimation of [Ni(salen)Ln(hfa)$_3$], Ln = Y, Gd. *Eur. J. Inorg. Chem.* **1998**, *8*, 1169–1174. [CrossRef]
27. Pointillart, F.; Bernot, K.; Sessoli, R.; Gatteschi, D. Effects of 3d–4f magnetic exchange interactions on the dynamics of the magnetization of Dy(III)–M(II)–Dy(III) trinuclear clusters. *Chem. Eur. J.* **2007**, *13*, 1602–1609. [CrossRef] [PubMed]
28. Ramade, I.; Kahn, O.; Jeannin, Y.; Robert, F. Design and magnetic properties of a magnetically isolated $Gd^{III}Cu^{II}$ pair. Crystal structures of [Gd(hfa)$_3$Cu(salen)], [Y(hfa)$_3$Cu(salen)], [Gd(hfa)$_3$Cu(salen)(meim)], and [La(hfa)$_3$(H_2O)Cu(salen)][hfa = Hexafluoroacetylacetonato, salen = *N*,*N*′-Ethylenebis (salicylideneaminato), meim = 1-Methylimidazole]. *Inorg. Chem.* **1997**, *36*, 930–936.
29. Rogachev, A.Y.; Mironov, A.V.; Nemukhin, A.V. Experimental and theoretical studies of the products of reaction between Ln(hfa)$_3$ band Cu (acac)$_2$ (Ln = La, Y; acac = acetylacetonate, hfa = hexafluoroacetylacetonate). *J. Mol. Struct.* **2007**, *831*, 46–54. [CrossRef]
30. Yamaguchi, T.; Sunatsuki, Y.; Ishida, H.; Kojima, M.; Akashi, H.; Re, N.; Matsumoto, N.; Pochaba, A.; Mrozinski, J. Synthesis, structures, and magnetic properties of face-sharing heterodinuclear Ni(II)–Ln(III) (Ln = Eu, Gd, Tb, Dy) complexes. *Inorg. Chem.* **2008**, *47*, 5736–5745. [CrossRef] [PubMed]
31. Yi, X.; Calvez, G.; Daiguebonne, C.; Guillou, O.; Bernot, K. Rational organization of lanthanide-based smm dimers into three-dimensional networks. *Inorg. Chem.* **2015**, *54*, 5213–5219. [CrossRef] [PubMed]

32. Wang, C.; Lin, S.-Y.; Shi, W.; Cheng, P.; Tang, J. Exploiting verdazyl radicals to assemble 2p–3d–4f one-dimensional chains. *Dalton Trans.* **2015**, *44*, 5364–5368. [CrossRef] [PubMed]
33. Wang, X.; Li, C.; Sun, J.; Li, L. Nitronyl nitroxide based 2p–3d–4f chains with the magnetocaloric effect and slow magnetic relaxation. *Dalton Trans.* **2015**, *44*, 18411–18417. [CrossRef] [PubMed]
34. Gatteschi, D.; Sessoli, R.; Villain, J. *Molecular Nanomagnets*; Oxford University Press: Oxford, UK, 2006.
35. Hansen, S.; Lehmann, G. EPR of Fe^{3+} in acetylacetonates. *Appl. Magn. Reson.* **1990**, *1*, 47–53. [CrossRef]
36. Pritchard, B.; Autschbach, J. Theoretical investigation of paramagnetic NMR shifts in transition metal acetylacetonato complexes: Analysis of signs, magnitudes, and the role of the covalency of ligand–metal bonding. *Inorg. Chem.* **2012**, *51*, 8340–8351. [CrossRef] [PubMed]
37. Dreiser, J.; Pedersen, K.S.; Piamonteze, C.; Rusponi, S.; Salman, Z.; Ali, M.E.; Schau-Magnussen, M.; Thuesen, C.A.; Piligkos, S.; Weihe, H. Direct observation of a ferri-to-ferromagnetic transition in a fluoride-bridged 3d–4f molecular cluster. *Chem. Sci.* **2012**, *3*, 1024–1032. [CrossRef]
38. Cremades, E.; Gómez-Coca, S.; Aravena, D.; Alvarez, S.; Ruiz, E. Theoretical study of exchange coupling in 3d-Gd complexes: Large magnetocaloric effect systems. *J. Am. Chem. Soc.* **2012**, *134*, 10532–10542. [CrossRef] [PubMed]
39. Pedersen, K.S.; Sørensen, M.A.; Bendix, J. Fluoride-coordination chemistry in molecular and low-dimensional magnetism. *Coord. Chem. Rev.* **2015**, *299*, 1–21. [CrossRef]
40. Holmberg, R.J.; Ungur, L.; Korobkov, I.; Chibotaru, L.; Murugesu, M. Observation of unusual slow-relaxation of the magnetisation in a Gd–EDTA chelate. *Dalton Trans.* **2015**, *44*, 20321–20325. [CrossRef] [PubMed]
41. Stamatatos, T.C.; Wernsdorfer, W.; Christou, G. Enhancing the Quantum Properties of Manganese–Lanthanide Single-Molecule Magnets: Observation of Quantum Tunneling Steps in the Hysteresis Loops of a $\{Mn_{12}Gd\}$ Cluster. *Angew. Chem. Int. Ed.* **2009**, *48*, 521–524. [CrossRef] [PubMed]
42. Lucaccini, E.; Sorace, L.; Perfetti, M.; Costes, J.-P.; Sessoli, R. Beyond the anisotropy barrier: Slow relaxation of the magnetization in both easy-axis and easy-plane Ln(trensal) complexes. *Chem. Commun.* **2014**, *50*, 1648–1651. [CrossRef] [PubMed]
43. Bernot, K.; Pointillart, F.; Rosa, P.; Etienne, M.; Sessoli, R.; Gatteschi, D. Single molecule magnet behaviour in robust dysprosium–biradical complexes. *Chem. Commun.* **2010**, *46*, 6458–6460. [CrossRef] [PubMed]
44. Richardson, M.F.; Wagner, W.F.; Sands, D.E. Rare-earth trishexafluoroacetylacetonates and related compounds. *J. Inorg. Nucl. Chem.* **1968**, *30*, 1275–1289. [CrossRef]
45. Glidewell, C. *Inorganic Experiments*; Wiley-VCH: Weinheim, Germany, 2003.
46. Liu, R.; Van Rooyen, P.H.; Conradie, J. Geometrical isomers of tris (β-diketonato) metal(III) complexes for M = Cr or Co: Synthesis, X-ray structures and DFT study. *Inorg. Chim. Acta* **2016**, *447*, 59–65. [CrossRef]
47. Bain, G.A.; Berry, J.F. Diamagnetic corrections and pascal's constants. *J. Chem. Educ.* **2008**, *85*, 532–536. [CrossRef]
48. Stoll, S.; Schweiger, A. Easyspin, a comprehensive software package for spectral simulation and analysis in EPR. *J. Magn. Reson.* **2006**, *178*, 42–55. [CrossRef] [PubMed]